Scientia Iranica B (2019) 26(4), 2431–2440

SCIENTIA IRANICA

Sharif University of Technology
Scientia Iranica
Transactions B: Mechanical Engineering
http://scientiairanica.sharif.edu

An analytical study of mechanical behavior of human arteries: A nonlinear elastic double-layer model

A. Safi Jahanshahi[a,b] and A.R. Saidi[a,*]

a. *Department of Mechanical Engineering, Shahid Bahonar University, Kerman, Iran.*
b. *Department of Mechanical Engineering, Sirjan University of Technology, Sirjan, Iran.*

Received 5 December 2017; received in revised form 3 March 2018; accepted 15 September 2018

KEYWORDS
Artery;
Analytical solution;
Non-linear elasticity;
Large deformation;
Biaxial test.

Abstract. The aim of this article is providing an analytical solution for stress and deformation of human arteries. The artery is considered as a long homogeneous isotropic cylinder. Hyperelastic, incompressible stress-strain behavior was applied by adopting a classical Mooney-Rivlin material model. The elastic constants of the arteries were calculated by using the reported results of biaxial test. The analysis was based on both single- and double-layer arterial wall models, and radial and circumferential stress distributions in the minimum and maximum blood pressures were calculated. Variations of radii due to internal pressure within the arteries were found; they were in a good agreement with the experimental results. The results containing the changes in diameter and thickness together with the stress distribution for both single- and double-layer models are plotted. It will be shown that the major difference between the single- and double-layer models is in their stress distributions. The circumferential stress distribution for different ages of human is plotted, which shows that the stress increases with increase in the age due to decrease in the flexibility of the artery. It is also shown that, although the inner layer of the artery is softer than its outer layer, the maximum stresses occur in the inner layer.

1. Introduction

The structure and function of arteries change throughout the lifetime of humans and animals [1]. Blood vessel can be considered as a long cylinder of which the internal pressure varies between a minimum and a maximum. The internal pressure is caused by systolic and diastolic blood pressures due to contraction of the heart muscle and blood flow through the arteries. Arteries and veins in different regions of body show different characteristics. Artery walls are mainly composed of three layers of tunica intima, tunica media, and tunica adventitia (Figure 1) [2].

The inner layer is covered by a layer of endothelial cells and it is very thin. These cells, through mechanical and electrochemical connections with each other, make an internal membrane for the blood vessels. In fact, this membrane forms a boundary between the blood and the vessel wall. Endothelial cells are formed of collagen, fibronectin, and laminin [3-6].

The middle layer or the main wall of the arteries includes muscle cells, elastin, and collagen fibers [3,5,6]. It has the greatest volume and is responsible for most of the arterial properties, consisting of a three-dimensional network of smooth muscle cells, elastin, and bundles of collagen fibrils (type I about 30% and type III about 70%) [6-8]. Adventitia refers to the outermost connective tissue covering organs, vessels, or any other structure. The outermost layer of artery

*. *Corresponding author. Tel.: +98 34 32114041; Fax: +98 34 32120964*
E-mail addresses: jahanshahi@sirjantech.ac.ir (A. Safi Jahanshahi); saidi@uk.ac.ir (A.R. Saidi);

doi: 10.24200/sci.2018.5707.1433

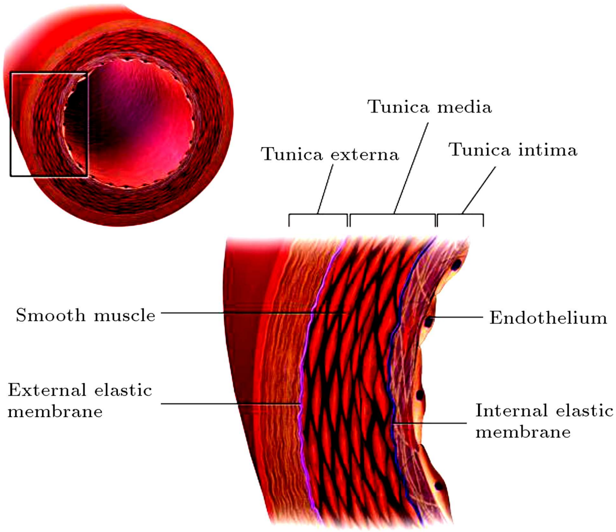

Figure 1. Cross-section of an artery and vein composed of the endothelium, tunica intima, tunica media, and tunica adventitia [2].

is called adventitia, because it is considered extraneous to the artery. It consists of type I collagen, nerves, fibroblast (a cell capable of forming collagen fiber), and some elastin fibers [9]. It is also believed that adventitia has the greatest contribution to elastic modulus of vessel wall [10].

Tests performed on live tissues are divided in two categories, namely in vitro and in vivo. Garcıa-Herrera et al. [11] characterized the human aorta under in-vitro and in-vivo conditions. Carew et al. [12], by using in-vitro experiments, showed that for most of the practical purposes, arteries might be considered incompressible. Karimi et al. [13] investigated the linear and nonlinear mechanical properties of human artery using a series of uniaxial tensile tests. Akhtar [14], by using in-vitro experiments and tensile testing, studied the biomechanical properties of arterial tissue. Vaishnav et al. [15], by using in-vitro experiments, showed that the wall tissue could be considered incompressible. Using the results of in-vivo tests, Hudetz [7] developed different continuum models for anisotropic, incremental elastic, nonlinear viscoelastic, and time-dependent active responses of arterial walls. In macroscopic analyses, the whole artery wall can be considered as a long, homogenous, isotropic, and incompressible material [7,12,15-17]. The stability behavior of thoracic aorta was investigated with two boundary conditions by Rastgar-Agah et al. [18], representing two extreme cases of in-vivo constraints.

A suitable mechanical model that is capable of predicting the artery behavior can be useful in the prevention and treatment of some artery diseases. In addition, reliable artery behavior prediction is an important step toward the production of some artificial tissues. Taghizadeh et al. [19] examined different strain energy functions to express the mechanical behavior of soft tissues. Von Maltzahn et al. [20-22] proposed a two-layer cylindrical model to describe the nonlinear properties of carotid arteries. Holzapfel and Ogden [23] and Holzapfel and Weizsacker [24] considered a two-layer, anisotropic mechanical model for arteries and used the Neo-Hookian model to express the matrix material.

Numerous biomechanical studies have idealized the three-dimensional wall as a membrane (or two-dimensional surface) [25-28].

Constitutive equations for the arterial wall can further be categorized by the types of biological processes. Deformations of live tissues are very large and their mechanical behavior is nonlinear [29]. For mathematical modeling of arteries, they can be considered as long single- or double-layer cylinders [20-24]. Safi Jahanshahi and Saidi [29] examined the mechanical behavior of human arteries by a single-layer isotropic model using biaxial stress test results.

In most studies of mechanical modeling, the artery wall is assumed as a thin cylinder [22-24,30-33], which is not an accurate assumption.

In this paper, a nonlinear elastic, thick, long cylindrical shell model has been used to predict the stress and deformation of human arteries under internal pressure. Since the intima layer is so thin and it does not have a considerable role in creating the stresses, the artery has been modeled as a double-layer cylindrical shell. Using a biaxial stress test, the Mooney-Rivlin elastic constants for this model have been calculated. Through an analytical solution, the radial and circumferential stress distributions in the minimum and maximum blood pressures have been found. Numerical results containing the changes in diameter and thickness together with the stress distribution for both single- and double-layer models have been plotted. The circumferential stress distributions for different human ages have been depicted, which show that the stresses increase with increase in human age.

2. Constitutive equations

The strain energy function, W, for a homogeneous material depends only on the deformation gradient tensor, $\boldsymbol{F}$. If there is no internal constraint, such as incompressibility, the nominal stress is work conjugate to the deformation gradient and given simply by [7]:

$$\boldsymbol{S}=\frac{\partial W}{\partial \boldsymbol{F}}, \tag{1}$$

where $\boldsymbol{S}$ is the nominal stress. For an incompressible material, Eq. (1) will be written as:

$$\boldsymbol{S}=\frac{\partial W}{\partial \boldsymbol{F}}-p\boldsymbol{F}^{-1}, \qquad J=\det \boldsymbol{F}=1, \tag{2}$$

where p is the Lagrange multiplier associated with the compressibility constraint and J stands for Jacobian. From Eq. (1), the Cauchy stress tensor, $\boldsymbol{T}$, can be written as:

$$\boldsymbol{T} = J\boldsymbol{F}^{-1}\frac{\partial W}{\partial \boldsymbol{F}}. \tag{3}$$

For an incompressible material, the above equation is modified to:

$$\boldsymbol{T} = \boldsymbol{F}^{-1}\frac{\partial W}{\partial \boldsymbol{F}} - p\boldsymbol{I}, \qquad \det \boldsymbol{F} = 1. \tag{4}$$

An important consequence of isotropy is that the Cauchy stress, $\boldsymbol{T}$, has the same eigenvectors as the left stretch tensor, $\boldsymbol{V}$. Thus, we can write:

$$\boldsymbol{T} = \sum_{i=1}^{3} t_i v^{(i)} \otimes v^{(i)}, \tag{5}$$

where t_i represents the principal values of the Cauchy stress tensor and the symbol $\otimes$ refers to the tensor product. Then:

$$Jt_i = \lambda_i \frac{\partial W}{\partial \lambda_i}, \qquad i = 1,2,3, \tag{6}$$

where λ_i represents the principal stretches. For an incompressible material, Eq. (6) can be written as:

$$t_i = \lambda_i \frac{\partial W}{\partial \lambda_i} - p, \quad \lambda_1\lambda_2\lambda_3 = 1, \quad i = 1,2,3. \tag{7}$$

Using Eq. (7) and having the energy function, W, the principal stresses can be found for incompressible materials.

3. Biaxial stress test

Biaxial mechanical tests are required to quantify mechanical properties of hyperelastic materials. Zemánek et al. [34] designed and produced an experimental rig for biaxial testing of hyperelastic materials (elastomers and soft tissues). The testing rig consisted of a bedplate carrying two orthogonal ball screws equipped with force gauges, two servo motors, and four carriages ensuring symmetric biaxial deformation of the specimen as well as a programmable CCD camera located on a support stand [34]. They presented the procedure of biaxial tension tests for aortic walls.

A pure homogeneous deformation, in general form, can be written as [23]:

$$x_1 = \lambda_1 X_1, \quad x_2 = \lambda_2 X_2, \quad x_3 = \lambda_3 X_3. \tag{8}$$

The deformation gradient tensor will then be found as:

$$\boldsymbol{F} = \begin{bmatrix} \lambda_1 & 0 & 0 \\ 0 & \lambda_2 & 0 \\ 0 & 0 & \lambda_3 \end{bmatrix}. \tag{9}$$

Imposing the incompressibility on Eq. (9) gives:

$$\boldsymbol{F} = \begin{bmatrix} \lambda_1 & 0 & 0 \\ 0 & \lambda_2 & 0 \\ 0 & 0 & \lambda_1^{-1}\lambda_2^{-1} \end{bmatrix},$$

$$\boldsymbol{B} = \boldsymbol{F}\boldsymbol{F}^T = \begin{bmatrix} \lambda_1^2 & 0 & 0 \\ 0 & \lambda_2^2 & 0 \\ 0 & 0 & \lambda_1^{-2}\lambda_2^{-2} \end{bmatrix}, \tag{10}$$

where $\boldsymbol{B}$ stands for the left Cauchy-Green deformation tensor. The invariants of $\boldsymbol{B}$, according to the principal stretches, are considered as:

$$I_1 = \lambda_1^2 + \lambda_2^2 + \lambda_3^2, \quad I_2 = \lambda_2^2\lambda_3^2 + \lambda_3^2\lambda_1^2 + \lambda_1^2\lambda_2^2,$$

$$I_3 = \lambda_1^2\lambda_2^2\lambda_3^2. \tag{11}$$

Enforcing the compressibility condition, Eq. (11) can be rewritten as:

$$I_1 = \lambda_1^2 + \lambda_2^2 + \lambda_1^{-2}\lambda_2^{-2},$$

$$I_2 = \lambda_1^{-2} + \lambda_2^{-2} + \lambda_1^2\lambda_2^2, \quad I_3 = 1. \tag{12}$$

The strain energy function $\widehat{W}$ is defined as:

$$\widehat{W}(\lambda_1, \lambda_2) = W(\lambda_1, \lambda_2, \lambda_1^{-1}\lambda_2^{-1}). \tag{13}$$

Omitting p from Eq. (7), we can write:

$$t_1 - t_3 = \lambda_1 \frac{\partial \widehat{W}}{\partial \lambda_1}, \qquad t_2 - t_3 = \lambda_2 \frac{\partial \widehat{W}}{\partial \lambda_2}. \tag{14}$$

For biaxial test, we have $t_3 = 0$; thus, in this case, the above equations slightly reduce to:

$$t_1 = \lambda_1 \frac{\partial \widehat{W}}{\partial \lambda_1}, \qquad t_2 = \lambda_2 \frac{\partial \widehat{W}}{\partial \lambda_2}. \tag{15}$$

Let us define $W_1 = \frac{\partial \widehat{W}}{\partial I_1}$ and $W_2 = \frac{\partial \widehat{W}}{\partial I_2}$. Thus, we can write:

$$W(I_1, I_2) \equiv \widehat{W}(\lambda_1, \lambda_2). \tag{16}$$

Eq. (15) then reduces to:

$$t_1 = \lambda_1\left[\frac{\partial \widehat{W}}{\partial I_1}\frac{\partial I_1}{\partial \lambda_1} + \frac{\partial \widehat{W}}{\partial I_2}\frac{\partial I_2}{\partial \lambda_1}\right] = 2(\lambda_1^2 - \lambda_1^{-2}\lambda_2^{-2})$$

$$(W_1 + \lambda_2^2 W_2). \tag{17}$$

Similarly, t_2 can be found as:

$$t_2 = 2(\lambda_2^2 - \lambda_1^{-2}\lambda_2^{-2})(W_1 + \lambda_1^2 W_2). \tag{18}$$

Solving these equations for W_1 and W_2 yields:

$$W_1 = \frac{\lambda_1^2 t_1}{2(\lambda_1^2-\lambda_2^2)(\lambda_1^2-\lambda_3^2)} - \frac{\lambda_2^2 t_2}{2(\lambda_1^2-\lambda_2^2)(\lambda_2^2-\lambda_3^2)},$$

$$W_2 = \frac{t_2}{2(\lambda_1^2-\lambda_2^2)(\lambda_2^2-\lambda_3^2)} - \frac{t_1}{2(\lambda_1^2-\lambda_2^2)(\lambda_1^2-\lambda_3^2)}. \quad (19)$$

For a Mooney-Rivlin material, the Helmholtz free energy function is [21]:

$$W = c_1(I_1-3)+c_2(I_2-3). \quad (20)$$

By comparing Eqs. (16) and (20), we have:

$$W_1 = c_1, \quad W_2 = c_2. \quad (21)$$

It means that by a biaxial test, the Mooney-Rivlin material constants can be specified. In this research, the material constants c_1 and c_2 are found using biaxial test results reported by Mohan and Melvin [35] and Eq. (19).

4. Mechanical analyses of artery

The artery wall is considered as a homogenous and isotropic cylinder under inflation and tension. For such a cylinder, the deformations field can be considered as [36]:

$$r = r(R), \qquad \theta = \Theta, \qquad z = Z/D, \quad (22)$$

where r, θ, and z are the cylindrical coordinate system in the current configuration and $\lambda_z = 1/D$ is stretch along the cylinder. For deformation field (22), the components of the deformation gradient tensor are given by:

$$\boldsymbol{F} = \begin{bmatrix} r' & 0 & 0 \\ 0 & r/R & 0 \\ 0 & 0 & 1/D \end{bmatrix}, \quad (23)$$

where $r' = dr/dR$. By satisfying the incompressibility condition, $\det\boldsymbol{F} = 1$, we have:

$$rr' = RD. \quad (24)$$

Solving Eq. (24) yields:

$$r^2 = DR^2 + A, \quad (25)$$

where A is an unknown constant, which has to be determined.

For a nonlinear elastic material, the constitutive equation is [37]:

$$\boldsymbol{T} = -p\boldsymbol{I} + c_1\boldsymbol{B} + c_2\boldsymbol{B}^{-1}, \quad (26)$$

where $\boldsymbol{T}$ is the Cauchy stress tensor, p is an unknown constant that appears in incompressibility condition, $\boldsymbol{I}$ is the identity tensor, and the constants c_1 and c_2 are the Mooney-Rivlin material constants, which can be determined using the biaxial test. For deformation field (22), the normal components of Cauchy stress tensor can be written as:

$$T_{rr} = -p + c_1\frac{D^2R^2}{r^2} + c_2\frac{r^2}{D^2R^2}, \quad (27)$$

$$T_{\theta\theta} = -p + c_1\frac{r^2}{R^2} + c_2\frac{R^2}{r^2}, \quad (28)$$

$$T_{zz} = -p + c_1\frac{1}{D^2} + c_2D^2. \quad (29)$$

In Eqs. (25) and (27)-(29), if constants p, D, and A are known, the stress distribution is completely known and the problem is completely solved. The equilibrium equation in r-direction is:

$$\frac{dT_{rr}}{dr} + \frac{1}{r}(T_{rr}-T_{\theta\theta}) = 0. \quad (30)$$

For a single-layer cylinder, the boundary conditions can be written as:

$$T_{rr}(r_{\text{in}}) = -P_{\text{in}}, \qquad T_{rr}(r_{\text{ou}}) = -P_{\text{ou}}, \quad (31)$$

$$F_a = 2\pi\int_{r_{\text{in}}}^{r_{\text{ou}}} T_{zz}r\,dr, \quad (32)$$

where P_{in} and P_{ou} are the inner and outer pressures of the cylinder and F_a is the axial force. Solving Eq. (30), using boundary conditions (31), and changing the internal radius to radius, we have:

$$T_{rr}(r) = -P_{\text{in}} - c_1\int_{r_{\text{in}}}^{r}\left(\frac{D^2R^2}{r^3} - \frac{r}{R^2}\right)dr - c_2\int_{r_{\text{in}}}^{r}\left(\frac{r}{D^2R^2} - \frac{R^2}{r^3}\right)dr. \quad (33)$$

By integrating and performing some mathematical operations, Eq. (33) can be written as:

$$T_{rr}(r) = -P_{\text{in}} - \left(c_1D - \frac{c_2}{D}\right)\left[\ln(r) + \frac{1}{2}\frac{A}{r^2} - \frac{1}{2}\ln(r^2-A)\right]_{r_{\text{in}}}^{r}. \quad (34)$$

By letting $r = r_{\text{ou}}$ in Eq. (34) and assuming that the external pressure is equal to zero, the following relationship between two constants A and D can be found:

$$0=-P_{\mathrm{in}}-(c_1D-\frac{c_2}{D})\Big[\ln(r)+\frac{1}{2}\frac{A}{r^2}-\frac{1}{2}\ln(r^2-A)\Big]_{r_{\mathrm{in}}}^{r_{\mathrm{ou}}}. \quad (35)$$

In addition, by comparing Eq. (35) and (27), the unknown constant p can be found in terms of the unknown constants A and D as follows:

$$p=+P_{\mathrm{in}}+c_1D\left(\frac{r_{\mathrm{ou}}^2-A}{r_{\mathrm{ou}}^2}\right)+\frac{c_2}{D}\left(\frac{r_{\mathrm{ou}}^2}{r_{\mathrm{ou}}^2-A}\right)+\left(c_1D-\frac{c_2}{D}\right)\Big[\ln(r)+\frac{1}{2}\frac{A}{r^2}-\frac{1}{2}\ln(r^2-A)\Big]_{r_{\mathrm{in}}}^{r_{\mathrm{ou}}}. \quad (36)$$

Furthermore, using the boundary condition (32), we have:

$$F_a=2\pi\int_{r_{\mathrm{in}}}^{r_{\mathrm{ou}}}\left(-p+c_1\frac{1}{D^2}+c_2D^2\right)rdr. \quad (37)$$

Substituting p from Eq. (36) into (37) and integrating them yield:

$$F_a=\pi\left[\begin{array}{l}-P_{\mathrm{in}}-c_1D\left(\frac{r_{\mathrm{ou}}^2-A}{r_{\mathrm{ou}}^2}\right)-\frac{c_2}{D}\left(\frac{r_{\mathrm{ou}}^2}{r_{\mathrm{ou}}^2-A}\right)-\left(c_1D-\frac{c_2}{D}\right)\times\\ \left[\ln(r)+\frac{1}{2}\frac{A}{r^2}-\frac{1}{2}\ln\left(r^2-A\right)\right]_{r_{\mathrm{in}}}^{r_{\mathrm{ou}}}+c_1\frac{1}{D^2}+c_2D^2\end{array}\right](r_{\mathrm{ou}}^2-r_{\mathrm{in}}^2). \quad (38)$$

By solving Eqs. (35) and (38), the constants A and D will be found and finally, the stress distribution will be fully determined.

As previously mentioned, the arterial wall consists of two main layers, namely media and adventitia. Thus, in order to have a more accurate model of the artery, it is considered as a double-layer cylinder. The boundary conditions for this model are:

$$T_{rr}(r_{\mathrm{in}})=-P_{\mathrm{in}}, \qquad T_{rr}(r_{\mathrm{ou}})=-P_{\mathrm{ou}}, \quad (39)$$

$$F_{\mathrm{a}}=2\pi\left(\int_{r_{\mathrm{in}}}^{r_1}T_{zz}rdr+\int_{r_1}^{r_{\mathrm{in}}}T_{zz}rdr\right), \quad (40)$$

where r_1 is the inner radius of the adventitia (which is equal to the outer radius of the media). By satisfying the boundary conditions (39) in Eq. (27), we can write:

$$T_{rr}(r_1)=-P_{\mathrm{in}}-\left(c_{1m}D_m-\frac{c_{2m}}{D_m}\right)\left[\ln(r)+\frac{1}{2}\frac{A_m}{r^2}-\frac{1}{2}\ln(r^2-A_m)\right]_{r_{\mathrm{in}}}^{r_1}, \quad (41)$$

$$0=-P_{\mathrm{ou}}=-T_{rr}\left(r_1\right)-\left(c_{1a}D_a-\frac{c_{2a}}{D_a}\right)\left[\ln\left(r\right)+\frac{1}{2}\frac{A_a}{r^2}-\frac{1}{2}\ln\left(r^2-A_a\right)\right]_{r_1}^{r_{\mathrm{ou}}}, \quad (42)$$

where the indices m and a stand for media and adventitia, respectively, and A_m, A_a, D_a, and D_m are four unknown constants, which should be determined from the boundary conditions. Eliminating $T_{rr}(r_1)$ from Eqs. (41) and (42), we obtain:

$$-P_{\mathrm{ou}}=-\left\{-P_{\mathrm{in}}-\left(c_{1m}D_m-\frac{c_{2m}}{D_m}\right)\left[\ln(r)+\frac{1}{2}\frac{A_m}{r^2}-\frac{1}{2}\ln\left(r^2-A_m\right)\right]_{r_{\mathrm{in}}}^{r_1}\right\}-\left(c_{1a}D_a-\frac{c_{2a}}{D_a}\right)\left[\ln(r)+\frac{1}{2}\frac{A_m}{r^2}-\frac{1}{2}\ln(r^2-A_m)\right]_{r_1}^{r_{\mathrm{ou}}}. \quad (43)$$

This is a relationship between the constants A_m, A_a, D_a, and D_m. By adopting the same procedure as the previous one, for a double-layer model, we can write:

$$p_m=+P_{\mathrm{in}}+c_{1m}D_m\left(\frac{r_1^2-A_m}{r_1^2}\right)+\frac{c_{2m}}{D_m}\left(\frac{r_1^2}{r_1^2-A_m}\right)+\left(c_{1m}D_m-\frac{c_{2m}}{D_m}\right)\left[\ln(r)+\frac{1}{2}\frac{A_m}{r^2}-\frac{1}{2}\ln(r^2-A_m)\right]_{r_{\mathrm{in}}}^{r_1}, \quad (44)$$

$$p_a=+P_{\mathrm{ou}}+c_{1a}D_a\left(\frac{r_{\mathrm{ou}}^2-A_a}{r_{\mathrm{ou}}^2}\right)+\frac{c_{2a}}{D_a}\left(\frac{r_{\mathrm{ou}}^2}{r_{\mathrm{ou}}^2-A_a}\right)+\left(c_{1a}D_a-\frac{c_{2a}}{D_a}\right)\left[\ln(r)+\frac{1}{2}\frac{A_a}{r^2}-\frac{1}{2}\ln(r^2-A_a)\right]_{r_1}^{r_{\mathrm{ou}}}. \quad (45)$$

Now, by applying the boundary conditions, Eq. (40)

will be:

$$F_a = 2\pi\left\{\int_{r_{\text{in}}}^{r_1}\left(-p_m + c_{1m}\frac{1}{D_m^2} + c_{2m}D_m^2\right)rdr + \int_{r_1}^{r_{\text{ou}}}\left(-p_a + c_{1a}\frac{1}{D_a^2} + c_{2a}D_a^2\right)rdr\right\}. \tag{46}$$

Substituting Eqs. (44) and (45) into Eq. (46) and integrating them yield Eq. (47) as shown in Box I. On the other hand, the non-slip condition requires:

$$D_a = D_m = D^*, \tag{48}$$

$$A_a = A_m = A^*. \tag{49}$$

Finally, by solving Eqs. (43) and (47), simultaneously, and using Eqs. (48) and (49), the constants A^* and D^* can be obtained and the problem will be solved completely.

5. Results

First, using the experimental results of biaxial stress test carried out by Mohan and Melvin [35], the Mooney-Rivlin material constants for a single-layer artery at different ages, based on Eqs. (19), are calculated and presented in Table 1. All the numerical results are presented based on these material constants.

To show the accuracy of our analytical solution, in Figure 2, the results for changes in the inner radius versus the internal pressure have been presented and compared with the experimental results published by Von Maltzahn et al. [20].

Table 1. Mooney-Rivlin constants of the arteries in different ages.

Age (year)	c_2 (Pa)	c_1 (Pa)	A (mm^2)	D (mm/mm)
25	-3147	10396	30.718	0.729
49	-3421	11128	27.090	0.736
60	-5082	19400	24.361	0.742
87	-6175	22725	22.536	0.749

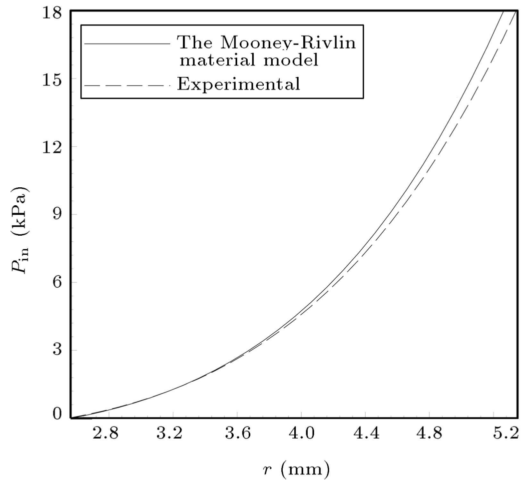

Figure 2. Comparison of the changes in the inner radius based on the results for the internal pressure by the presented model and the experimental results obtained by the tests of Von Maltzahn et al. [20].

From this figure, it can be found out that the results are in good agreement and therefore, our analytical solution is accurate.

Based on the single-layer model, the results for radial and circumferential stress distributions have been plotted in Figures 3 and 4, respectively.

The non-dimensional variation of the radial stress has been plotted based on the non-dimensional internal radius in Figure 3. The maximum blood pressure (or diastolic pressure) and the minimum blood pressure (or systolic pressure) are considered to be 75 and 150 mm Hg, respectively. The non-dimensional circumferential stress distribution versus the non-dimensional internal radius is depicted in Figure 4.

In order to find much more accurate results, a double-layer model is assumed. The Mooney-Rivlin material constants for media and adventitia layers of the artery at different ages are calculated and presented in Table 2.

$$f_a = \pi\left\{\left(-\left[\begin{matrix}P_{\text{in}} + c_{1m}D_m\left(\frac{r_1^2-A_m}{r_1^2}\right) + \frac{c_{2m}}{D_m}\left(\frac{r_1^2}{r_1^2-A_m}\right) + \\ \left(c_{1m}D_m - \frac{c_{2m}}{D_m}\right)\left[\ln(r) + \frac{1}{2}\frac{A_m}{r^2} - \frac{1}{2}\ln(r^2-A_m)\right]_{r_{\text{in}}}^{r_1}\end{matrix}\right] + c_{1m}\frac{1}{D_m^2} + c_{2m}D_m^2\right)(r_1^2 - r_{\text{in}}^2)\right.$$
$$\left. + \left(-\left[\begin{matrix}P_{\text{ou}} + c_{1a}D_a\left(\frac{r_{\text{ou}}^2-A_a}{r_{\text{ou}}^2}\right) + \frac{c_{2a}}{D_a}\left(\frac{r_{\text{ou}}^2}{r_{\text{ou}}^2-A_a}\right) + \\ \left(c_{1a}D_a - \frac{c_{2a}}{D_a}\right)\left[\ln(r) + \frac{1}{2}\frac{A_a}{r^2} - \frac{1}{2}\ln(r^2-A_a)\right]_{r_1}^{r_{\text{in}}}\end{matrix}\right] + c_{1a}\frac{1}{D_a^2} + c_{2a}D_a^2\right)(r_{\text{ou}}^2 - r_1^2)\right\}. \tag{47}$$

Box I

Table 2. Mooney-Rivlin constants for media and adventitia in different ages.

Age (year)	c_{1m} **(Pa)**	c_{2m} **(Pa)**	c_{1a} **(Pa)**	c_{2a} **(Pa)**	A^* **(mm^2)**	D^* **(mm/mm)**
25	16030	-4823	8150	-2467	30.604	0.745
49	19513	-5043	9725	-2849	29.156	0.751
60	27831	-7419	16421	-4446	26.982	0.772
87	30110	-8774	18725	-5014	24.732	0.785

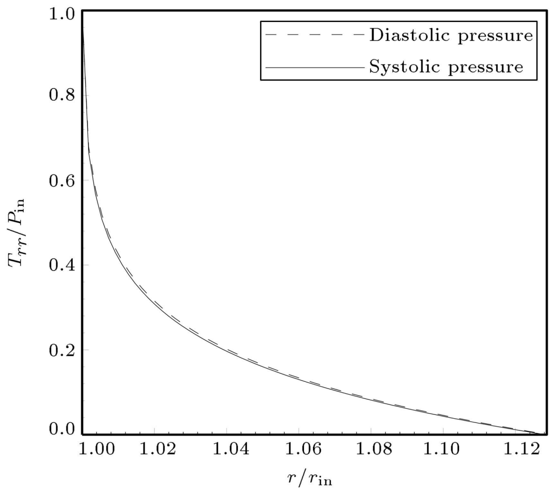

Figure 3. Non-dimensional radial stress distribution for systolic and diastolic blood pressures.

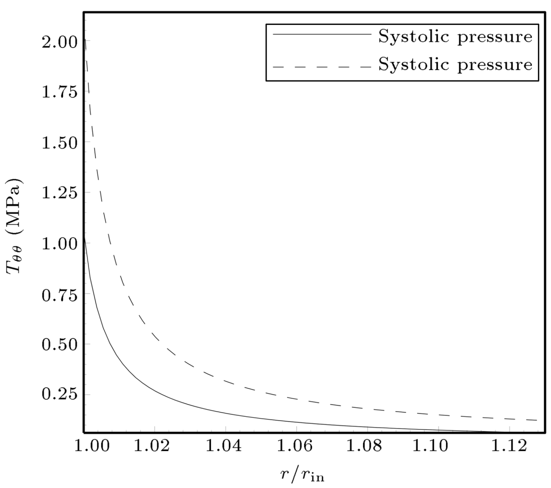

Figure 4. Non-dimensional circumferential stress distribution for systolic and diastolic blood pressures.

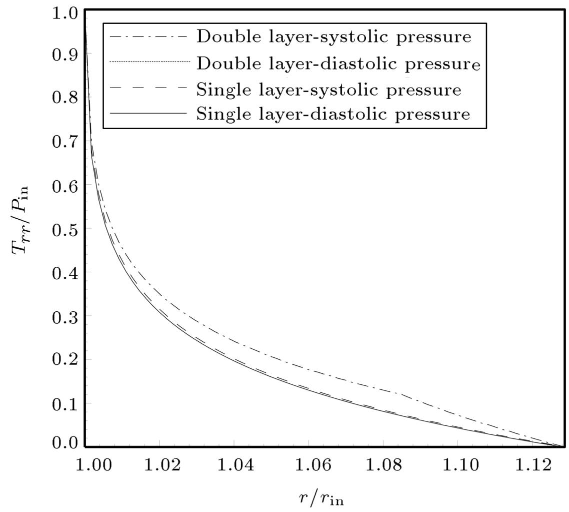

Figure 5. Non-dimensional radial stress distribution for systolic and diastolic blood pressures of both single- and double-layer models.

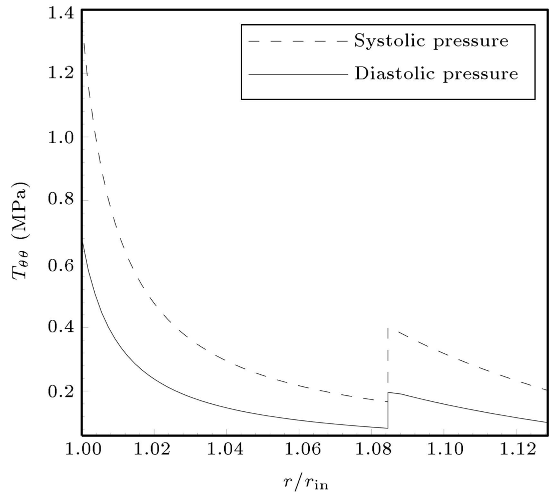

Figure 6. Non-dimensional circumferential stress distribution for systolic and diastolic blood pressures of the two-layer model.

The non-dimensional results for radial stress distribution based on the single- and double-layer model are depicted in Figure 5.

The results for non-dimensional circumferential stress distribution based on the double-layer model are depicted in Figure 6.

Variation of dimensionless inner radius is plotted versus the blood pressure in Figure 7.

The changes in outer radius are considerable, but smaller than those in the inner radius. This reveals that the thickness of the arteries decreases by increasing the internal pressure, as shown in Figure 8. It is clear that the change in thickness occurs due to incompressibility behavior of the artery.

In Table 3, the dimensionless inner radius changes

Table 3. Comparison of the changes in dimensionless inner radius based on the internal pressures of the single- and double-layer models.

P_{in} (kPa)	$r_{\text{in}}/R_{\text{in}}$ Single-layer	Double-layer	Difference (%)	$r_{\text{ou}}/R_{\text{ou}}$ Single-layer	Double-layer	Difference (%)
0	1	1	0	1	1	0
5	1.6048	1.6241	0.012	1.4763	1.4922	0.011
10	1.8418	1.8657	0.013	1.6827	1.7056	0.012
15	2.0141	2.0423	0.014	1.8362	1.8614	0.013
20	2.1379	2.1699	0.015	1.9458	1.9741	0.014

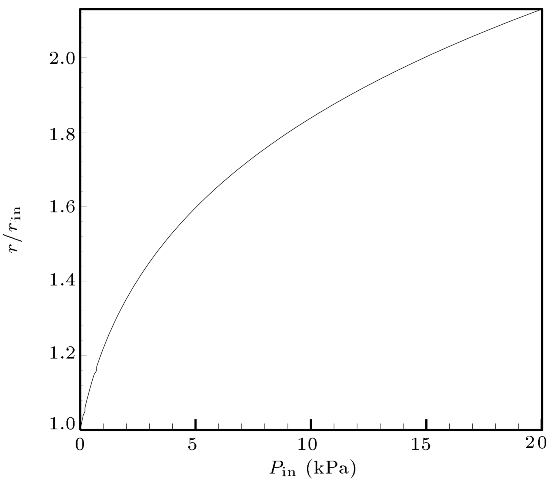

Figure 7. Dimensionless inner radius versus internal pressure.

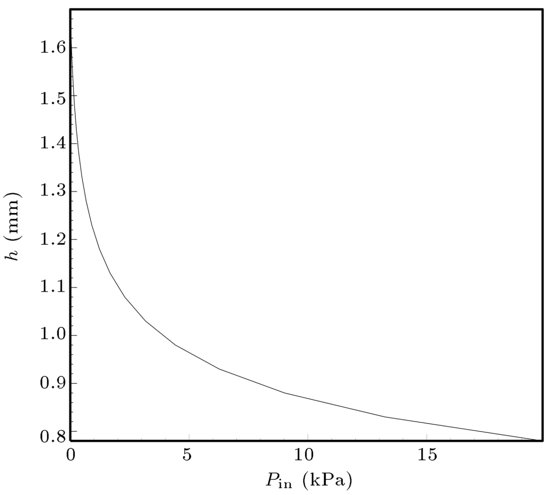

Figure 8. Thickness changes versus internal pressure.

versus the internal pressure based on single- and double-layer models are compared.

It is observable that the results are very close to each other; therefore, the results of the single-layer model for inner radius changes are accurate.

In Table 4, the radial and circumferential stresses based on single- and double-layer models are compared.

Table 4. Comparison of the stresses of the single- and double-layer models.

r (mm)	T_{rr} (kPa) Single-layer	Double-layer	$T_{\theta\theta}$ (MPa) Single-layer	Double-layer
5.42	20.2175	20.2176	2.1150	1.6651
5.52	6.5791	6.7383	0.5725	0.4507
5.62	4.3555	4.8140	0.3386	0.2666
5.72	3.1097	3.7360	0.2441	0.1922
5.82	2.2310	2.9756	0.1929	0.1519
5.92	1.5476	2.3058	0.1609	0.3709
6.02	0.9861	1.4693	0.1389	0.2798
6.12	0.5087	0.7578	0.1230	0.2086

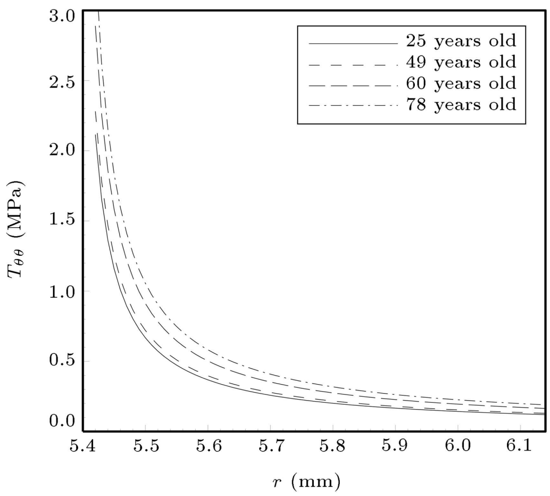

Figure 9. Circumferential stress distribution based on the radii for different ages.

Based on the double-layer model, the circumferential stress distribution along the radius at different ages for the internal pressure of 150 mm Hg is drawn in Figure 9.

6. Conclusions

This study revealed that the radial stress distribution was highly non-linear and varied between the blood pressure in the inner wall and zero at the outer wall. Also, it was found that the surfaces near the inner lining of artery had a more significant role in creating stress than the outer surfaces. As mentioned, the inner lining of the arteries was composed of the muscle cells, elastin fibers, and collagen; and the external layer was composed of collagen type I, nerve cells, and elastin fibers. Muscle cells had much greater elastic properties than collagen [3], which justified the resulting stress distribution. Moreover, it was concluded that the circumferential stresses close to the inner surface were very large and tapered off very rapidly.

By comparing the magnitudes of circumferential and radial stresses, it was found that the major stresses in mechanical analysis of arteries were circumferential, which were almost 100 times larger than the radial stresses.

Moreover, the internal radius expanded to more than twice its initial value, due to the internal pressure of about 15 kPa (112 mm Hg), which showed that the deformation was too large.

As the differences in stresses based on single- and double-layer models were noticeable, it was concluded that the single-layer model could not suitably predict the radial and circumferential stresses.

Finally, the circumferential stress in the arteries increased with increase in the age. For this reason, the flexibility of the artery was reduced.

References

1. Lakatta, E.G. "Central arterial aging and the epidemic of systolic hypertension and atherosclerosis", *Journal of the American Society of Hypertension*, **1**(5), pp. 302-340 (2007).
2. Staff, B.C. "Medical gallery of Blausen medical 2014", *WikiJournal of Medicine*, **1**(2), pp. 1-79 (2014).
3. Meyers, M.A., Chen, P.Y., Lin, A.Y.M., and Seki, Y. "Biological materials: structure and mechanical properties", *Progress in Materials Science*, **53**(1), pp. 1-206 (2008).
4. Jaffe, E.A. "Cell biology of endothelial cells", *Human Pathology*, **18**(3), pp. 234-239 (1987).
5. Cox, R.H. "Regional variation of series elasticity in canine arterial smooth muscles", *American Journal of Physiology-Heart and Circulatory Physiology*, **234**(5), pp. 542-551 (1978).
6. Karšaj, I. and Humphrey, J.D. "A multilayered wall model of arterial growth and remodeling", *Mechanics of Materials*, **44**, pp. 110-119 (2012).
7. Hudetz, A.G. "Continuum mechanical methods and models in arterial biomechanics", *Cardiovascular Physiology-Heart, Peripheral Circulation and Methodology, Advances in Physiological Science*, **8**, pp. 223-232 (2014).
8. Taber, L. "A model for aortic growth based on fluid shear and fiber stresses", *Journal of Biomechanical Engineering*, **120**(3), pp. 348-354 (1998).
9. Rachev, A. "A model of arterial adaptation to alterations in blood flow", *Journal of Elasticity and the Physical Science of Solids*, **61**(1-3), pp. 83-111 (2000).
10. Gleason, R., Taber, L., and Humphrey, J. "A 2-D model of flow-induced alterations in the geometry, structure, and properties of carotid arteries", *Journal of Biomechanical Engineering*, **126**(3), pp. 371-381 (2004).
11. García-Herrera, C.M., Celentano, D.J., Cruchaga, M.A., and Guinea, G.V. "Mechanical characterization of the human aorta: Experiments, modeling and simulation", in *Computational Modeling, Optimization and Manufacturing Simulation of Advanced Engineering Materials*, Ed., 4th Edn., Springer, pp. 151-202 (2016).
12. Carew, T.E., Vaishnav, R.N., and Patel, D.J. "Compressibility of the arterial wall", *Circulation Research*, **23**(1), pp. 61-68 (1968).
13. Karimi, A., Navidbakhsh, M., Alizadeh, M., and Shojaei, A. "A comparative study on the mechanical properties of the umbilical vein and umbilical artery under uniaxial loading", *Artery Research*, **8**(2), pp. 51-56 (2014).
14. Akhtar R. "In vitro characterisation of arterial stiffening: From the macro-to the nano-scale", *Artery Research*, **8**(1), pp. 1-8 (2014).
15. Vaishnav, R.N., Young, J.T., Janicki, J.S., and Patel, D.J. "Nonlinear anisotropic elastic properties of the canine aorta", *Biophysical Journal*, **12**(8), p. 1008 (1972).
16. Chuong, C. and Fung, Y. "Compressibility and constitutive equation of arterial wall in radial compression experiments", *Journal of Biomechanics*, **17**(1), pp. 35-40 (1984).
17. Papageorgiou, G. and Jones, N. "Physical modelling of the arterial wall. Part 2: Simulation of the non-linear elasticity of the arterial wall", *Journal of Biomedical Engineering*, **9**(3), pp. 216-221 (1987).
18. Rastgar-Agah, M., Laksari, K., Assari, S., and Darvish, K. "Mechanical Instability of Aorta due to Intraluminal Pressure", *International Journal of Applied Mechanics*, **8**(1), p. 1650002 (2016).
19. Taghizadeh, D., Bagheri, A., and Darijani, H. "On the hyperelastic pressurized thick-walled spherical shells and cylindrical tubes using the analytical closed-form solutions", *International Journal of Applied Mechanics*, **7**(2), pp. 115-127 (2015).
20. Von Maltzahn, W.W., Besdo, D., and Wiemer, W. "Elastic properties of arteries: a nonlinear two-layer cylindrical model", *Journal of Biomechanics*, **14**(6), pp. 389-397 (1981).

21. Von Maltzahn, W.W. "Stresses and strains in the cone-shaped carotid sinus and their effects on baroreceptor functions", *Journal of Biomechanics*, **15**(10), pp. 757-765 (1982).

22. Von Maltzahn, W.W., Warriyar, R.G., and Keitzer, W.F. "Experimental measurements of elastic properties of media and adventitia of bovine carotid arteries", *Journal of Biomechanics*, **17**(11), pp. 839-847 (1984).

23. Holzapfel, G.A. and Ogden, R.W., *Biomechanical Modelling at the Molecular, Cellular and Tissue Levels*, **508**, Springer Science & Business Media (2009).

24. Holzapfel, G.A. and Weizsäcker, H.W. "Biomechanical behavior of the arterial wall and its numerical characterization", *Computers in Biology and Medicine*, **28**(4), pp. 377-392 (1998).

25. Kroon, M. and Holzapfel, G.A. "A theoretical model for fibroblast-controlled growth of saccular cerebral aneurysms", *Journal of Theoretical Biology*, **257**(1), pp. 73-83 (2009).

26. Watton, P., Hill, N., and Heil, M. "A mathematical model for the growth of the abdominal aortic aneurysm", *Biomechanics and Modeling in Mechanobiology*, **3**(2), pp. 98-113 (2004).

27. Wulandana, R. and Robertson, A. "An inelastic multi-mechanism constitutive equation for cerebral arterial tissue", *Biomechanics and Modeling in Mechanobiology*, **4**(4), pp. 235-248 (2005).

28. Zasadzinski, J., Wong, A.B., Forbes, N., Braun, G., and Wu, G. "Novel methods of enhanced retention in and rapid, targeted release from liposomes", *Current Opinion in Colloid & Interface Science*, **16**(3), pp. 203-214 (2011).

29. Safi Jahanshahi, A. and Saidi, A. "Mechanical behavior of human arteries in large deformation using non-linear elasticity theory", *Modares Mechanical Engineering*, **15**(12), pp. 153-158 (2015).

30. Tsamis, A., Stergiopulos, N., and Rachev, A. "A structure-based model of arterial remodeling in response to sustained hypertension", *Journal of Biomechanical Engineering*, **131**(10), p. 101004 (2009).

31. Valent ın, A., Cardamone, L., Baek, S., and Humphrey, J. "Complementary vasoactivity and matrix remodelling in arterial adaptations to altered flow and pressure", *Journal of The Royal Society Interface*, **6**(32), pp. 293-306 (2009).

32. Wan, W., Hansen, L., and Gleason Jr, R.L. "A 3-D constrained mixture model for mechanically mediated vascular growth and remodeling", *Biomechanics and Modeling in Mechanobiology*, **9**(4), pp. 403-419 (2010).

33. Holzapfel, G.A. and Ogden, R.W. "Modelling the layer-specific three-dimensional residual stresses in arteries, with an application to the human aorta", *Journal of the Royal Society Interface*, pp. 290-357 (2009).

34. Zemánek, M., Burša, J., and Děták, M. "Biaxial tension tests with soft tissues of arterial wall", *Engineering Mechanics*, **16**(1), pp. 3-11 (2009).

35. Mohan, D. and Melvin, J.W. "Failure properties of passive human aortic tissue. II Biaxial tension tests", *Journal of Biomechanics*, **16**(1), pp. 31-44 (1983).

36. Batra, R. and Bahrami, A. "Inflation and eversion of functionally graded non-linear elastic incompressible circular cylinders", *International Journal of Non-Linear Mechanics*, **44**(3), pp. 311-323 (2009).

37. Rubin, D., Krempl, E., and Lai, W.M. *Introduction to Continuum Mechanics*, 3th Edn., pp. 314-347, Butterworth Heinemann, Woburn (1993).

Biographies

Amin Safi Jahanshahi was born in Sirjan, Iran, in 1978. He received his BSc in Solid Mechanics from Shahid Bahonar University of Kerman, Iran, in 2002, and his MSc in Applied Mechanics from Amir Kabir University of Technology, Iran, in 2005. Also, he obtained his PhD degree in Applied Mechanics from Shahid Bahonar University of Kerman, Iran, in 2017. He is currently an Assistant Professor at Sirjan University of Technology. He has been involved in teaching and research activities in the stress analyses areas at Sirjan University of Technology for the last ten years. His research interests include nonlinear continuum mechanics, constitutive modeling of hyperelastic materials, non-Linear elasticity, finite deformation, and plasticity.

Ali Reza Saidi was born in Rafsanjan, Iran, in 1970. He received his BSc in Solid Mechanics from Amir Kabir University of Technology, Iran, in 1996, and his MSc in Applied Mechanics from Sharif University of Technology, Iran, in 1998. Moreover, he obtained his PhD degree in Aerospace Structures from Sharif University of Technology, Iran, in 2003. He is currently a Professor at Shahid Bahonar University of Kerman. His research interests include nonlinear continuum mechanics, constitutive modeling of hyperelastic materials, non-linear elasticity, thermoelasticity, nanomechanics, finite deformation, and plasticity.